ACI MATERIALS JOURNAL TECHNICAL PAPER

Title no. 107-M70

Self-Healing Characterization of Engineered Cementitious Composite Materials

by Li-Li Kan, Hui-Sheng Shi, Aaron R. Sakulich, and Victor C. Li

This research investigates the self-healing behavior of engineered cementitious composite (ECC) materials. Crack characteristics, resonant frequency (RF) recovery, and the effect of wet-dry conditioning cycles were studied. Characterization of the self-healing products in ECC materials was carried out with an environmental scanning electron microscope-energy dispersive spectroscopy system (ESEM-EDS), transmission electron microscopy (TEM), Fourier transform infrared spectroscopy (FTIR), and X-ray diffraction (XRD). According to the experimental results, wet-dry conditioning cycles aid self-healing, most of which occurs before four to five cycles. The products of self-healing were identified as mainly C-S-H and calcite. These products almost completely bridge cracks less than 50 μm wide. Overall, the self-controlled tight crack width (CW) of ECC materials tailored for high-tensile ductility encourages robust self-healing behavior in both young and mature (3- and 90-day-old) ECC specimens, respectively.

Keywords: engineered cementitious composites; resonant frequency; self-healing; self-healing process and product.

INTRODUCTION

Cracks are inevitable during the life of a concrete structure. Cracks can be caused by loading, volumetric change due to high temperatures, creep, plastic settlement, shrinkage, or deterioration mechanisms such as alkali-silicate reaction and freezing-and-thawing cycles.[1] Cracks lower the durability of concrete structures by creating preferential paths for the penetration of potentially aggressive agents that may attack either the concrete itself or the reinforcing steel. The presence of cracks may also mechanically weaken the structure or lead to a loss of water-tightness and reduced stiffness. Therefore, the development of a new kind of cementitious material that can autogenously counter the effects of cracking by self-healing is highly desirable.

Self-healing generally refers to the long-known ability of a crack to diminish autogeneously in width over time. In 1836, the ability of small cracks in concrete to heal themselves in the presence of moisture was observed by the French Academy of Science.[2] Experimental investigation and practical experience have demonstrated[3-6] that the healing of cracks in cementitious materials leads to a gradual reduction of permeability over time for water flowing under a hydraulic gradient. In extreme cases, cracks can be completely sealed. Regardless of origin, self-healing leads to crack-closing, thus improving durability, permeability, and potentially mechanical properties.[3] This is important for watertight structures and for prolonging the service life of infrastructure. While self-sealing is widely studied, the ability of cracks to autogenously regain load-carrying capacity—true healing—has received limited attention.

Engineered cementitious composites (ECCs) are a class of ultra-ductile fiber-reinforced cementitious composites developed for applications in the construction industry.[7] ECCs have been optimized through the use of micromechanics to attain high-tensile ductility and tight microcrack width at moderate fiber contents (2 volume percent or less).[8-10] The extreme tensile strain capacity of ECCs (beyond 3%; refer to Fig. 1(a)) is several hundred times that of normal concrete, and ECC toughness is similar to that of aluminum alloys.[11] Figure 1(a) also shows that the crack widths (CWs) of ECCs can remain small—less than 60 μm (0.002 in.), even at large deformations. In previous studies,[1-3] controlling CWs has been found to promote self-healing behavior, which has recently been observed in ECCs.[12,13] In conventional concrete, CWs cannot

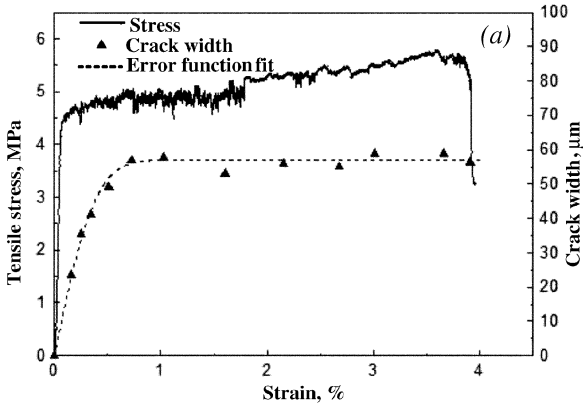

Fig. 1—(a) Typical tensile stress-strain curve and CW development of ECC; and (b) setup of uniaxial tensile loading. (Note: 1 MPa = 0.145 ksi.)

ACI Materials Journal, V. 107, No. 6, November-December 2010.
MS No. M-2010-022.R1 received January 20, 2010, and reviewed under Institute publication policies. Copyright © 2010, American Concrete Institute. All rights reserved, including the making of copies unless permission is obtained from the copyright proprietors. Pertinent discussion including authors' closure, if any, will be published in the September-October 2011 *ACI Materials Journal* if the discussion is received by June 1, 2011.

Li-Li Kan *is a Graduate Student in the Department of Material Science and Engineering at Tongji University, Shanghai, China. She received her BS from Kunming University of Science and Technology, Kunming, China, and her MS from Tongji University, Shanghai, China. Her research interests include new cementitious building materials.*

Hui-Sheng Shi *is a Professor in the Department of Material Science and Engineering at Tongji University. He received his BS and PhD from Tongji University and his MS from the China Building Materials Academy, Beijing, China. His research interests include high-performance cementitious materials and ecological cement-based materials.*

Aaron R. Sakulich *is a Postdoctoral Researcher in the Department of Civil and Environmental Engineering at the University of Michigan, Ann Arbor, MI. He received his BS and PhD from the Department of Materials Science and Engineering at Drexel University, Philadelphia, PA. His research interests include ecologically sustainable building materials and the preservation of cultural heritage.*

ACI member **Victor C. Li** *is a Professor in the Department of Civil and Environmental Engineering at the University of Michigan. He is a member of ACI Committee 544, Fiber-Reinforced Concrete. His research interests include the micromechanics of cementitious materials; the design, characterization, and application of high-ductility cement-based composites; and the materials-based development of sustainable infrastructure.*

Table 1—Mixture design proportion by weight for ECC specimen

	Components, wt. %						
Sample	Cement	Sand	Fly ash	HRWRA	Water	Fiber	*w/b*[*]
ECC	27	22	33	0.4	16	1.3	0.267

[*]Weight ratio of water-binder (cement + fly ash) material.

Table 2—Chemical compositions and physical properties of portland cement and fly ash

Chemical composition, %	Portland cement	Fly ash
CaO	61.80	5.57
SiO_2	19.40	59.50
Al_2O_3	5.30	22.20
Fe_2O_3	2.30	3.90
MgO	0.95	Not measured
SO_3	3.80	0.19
K_2O	1.10	1.11
Na_2O	0.20	2.75
Loss on ignition	2.10	0.21
Physical properties		
Specific gravity	3.15	2.18
Retained on 45 μm (0.002 in.), %	12.9	9.6
Water requirement, %	Not measured	93.4

be reliably controlled; therefore, it is not possible to produce consistent self-healing behavior. In ECCs, however, the steady-state CW is a tunable, intrinsic material property. A body of literature[14-19] concerning the self-healing of concrete exists, but specifics regarding ECCs are limited.[12] Most previous work focuses on the effects of self-healing such as reducing permeability,[13] as opposed to the chemistry of—and processes that promote—self-healing. In this paper, crack characteristics and resonant frequency (RF) recovery are used to verify self-healing, after which the chemical composition of healing products is reported.

RESEARCH SIGNIFICANCE

Yang et al.[13] studied the self-healing of ECCs exposed to different environments and found that exposure of crack-damaged specimens to wet-dry cycles was the most effective promoter of self-healing. It was also shown that RF recovery is directly related to the recovery of mechanical properties and therefore can be used as a method to quantify healing. This paper builds on that research by using RF to verify that self-healing is taking place and then providing the chemical and morphological characterization of the healing products. This information is lacking in the literature and will help lead to the design of ECCs with a robust self-healing ability and more durable, sustainable infrastructure that requires less maintenance, consumes fewer resources, and generates a lower carbon footprint.

EXPERIMENTAL INVESTIGATION

Raw materials

The mixture proportion of ECCs used in this study is shown in Table 1. Type I ordinary portland cement; fine silica sand, with an average grain size of 110 μm (0.004 in.); Class F normal fly ash, conforming to ASTM C618 requirements; polyvinyl alcohol (PVA) fibers; and a polycarboxylate-based high-range water-reducing admixture (HRWRA) were used. The chemical and physical properties of the portland cement and fly ash are shown in Table 2. The PVA fibers had an average diameter of 39 μm (0.0016 in.), an average length of 12 mm (0.5 in.), a tensile strength of 1600 MPa (232 ksi), a density of 1300 kg/m^3 (2192 lb/yd^3), an elastic modulus of 42.8 GPa (6200 ksi), and a maximum elongation of 6.0%. Due to the strongly hydrophilic nature of PVA, the fiber surfaces were coated with an oiling agent (1.2% by weight) to reduce the interfacial bond strength between the fiber and matrix.[20-22]

ECC material preparation

A series of coupon specimens measuring 300 x 76 x 12.5 mm (12 x 3.0 x 0.5 in.) was cast from a single batch of ECC prepared using a force-based 20 L (0.71 ft^3) capacity mixer. Specimens were demolded after 24 hours, covered with plastic sheets, and air-cured at laboratory temperature (20 ± 1°C [68 ± 1.8°F]) and relative humidity (RH) (50 ± 5%) until testing. Three- and 90-day-old specimens were studied. Direct uniaxial tensile loading was applied to these specimens (Fig. 1(b)) using a 25 kN (5.62 kip) capacity load frame under displacement control. A quasi-static loading speed of 0.0025 mm/s (0.0001 in./s) was used. Prior to loading, aluminum plates were glued to both ends of the coupon specimen to facilitate gripping. The ECC specimens were loaded to specified tensile deformations of 0.3, 0.5, 1.0, and 2.0%, producing different levels of microcrack damage. When the tensile strain reached the predetermined values, the load was released, and the specimens were removed to prepare for wet-dry cycles. Prior to wet-dry cycle conditioning, CWs in these specimens were measured in the unloaded state using a portable optical microscope over a gauge length of 100 mm (3.94 in.). Crack closure of approximately 15% during unloading has been reported[13]; therefore, all CW measurements reported herein were obtained in the unloaded state from along the centerline of the specimen.

Environmental exposure

After preloading, specimens were subjected to wet-dry cycles consisting of submerging the ECC specimens in water at 20°C (68°F) for 24 hours followed by drying the specimens in air at 20 ± 1°C (68 ± 1.8°F), 50 ± 5% RH for 24 hours. These cycles were meant to simulate cyclic outdoor environments such as rainy days followed by clear days. During each cycle, water was changed to prevent it from becoming saturated with leached calcium.

Self-healing product characterization

Longitudinal RF measurements based on ASTM C215 were carried out on coupon specimens to verify the presence of and quantify both the damage and self-healing in ECC materials. Samples for observation by an environmental scanning electron microscope (ESEM) equipped with an energy dispersive spectroscopy (EDS) system were prepared by cutting coupons into small cubes and affixing them to aluminum stubs. A conductive coating was not used. Samples for observation by an analytical electron microscope (AEM) were prepared by scratching the surface of the healed specimens with a razor. Further characterization was carried out by Fourier transform infrared spectroscopy (FTIR) in transmission mode (4 cm^{-1} scan resolution; 58 scans averaged). Finally, X-ray diffraction (XRD) experiments were carried out (C_u $k\alpha$ radiation with $\lambda = 0.154$ nm; 0.02-degree step size, and 2-second dwell time). Ninety-day-old samples were observed by ESEM, while 3-day-old samples were analyzed by transmission electron microscopy (TEM), XRD, and FTIR due to sample constraints. Though there may be some difference in the nature of the healing products in each type of sample, the results in the following paragraphs indicate strong similarities.

EXPERIMENTAL RESULTS AND DISCUSSION

Crack characteristics of preloaded ECC

Crack characteristics of the eight strain/age combination specimens investigated, including the number of cracks, average CW, and maximum CW are shown in Table 3. The total crack number includes all of the cracks, whereas the average CW is calculated using only CWs larger than 10 μm. Each point is an average of four measurements. As shown in Table 3, for specimens preloaded to 2.0%, the maximum CW is only 80 μm for 3-day-old samples and 70 μm for 90-day-old samples. The 90-day-old samples had a higher number of cracks but a lower average CW compared to the 3-day-old samples. This is likely due to the increase in chemical bonds (and thus debonding fracture energy) and frictional stress at the fiber/matrix interface in ECCs over time due to continued hydration. Future work will be carried out on single-fiber pullout tests to confirm and quantify this behavior.

RF recovery of ECC

Three- and 90-day-old samples were investigated to determine the effect of age on self-healing. Longitudinal RF was measured before and after uniaxial tensile preloading for each environmental conditioning cycle. Each data point is an average of three specimens. Figure 2 plots the RF ratio value of 3- and 90-day-old samples versus the preload strain level after 10 wet-dry cycles (10 cycles were chosen based on previous studies[12,13]). The RF ratio provides the change of RF in preloaded specimens calculated according to the following

$$\text{RF ratio} = \frac{RF_{preloaded}}{RF_{virgin}} \times 100\% \quad (1)$$

where $RF_{preloaded}$ is the RF value of the preloaded specimens with or without 10 wet-dry cycles and RF_{virgin} is the RF value of virgin specimens without preloading or wet-dry cycle exposure. Thus, the RF ratio value measures the amount of loss of RF due to crack damage for specimens without healing and the amount of recovery of RF for specimens with healing due to 10 cycles of wet-dry cycle exposure.

Table 3—Crack characteristics of preloaded ECC

Tensile strain	Total number of cracks	Number of cracks, >10 μm	Average CW, μm (in.)	Maximum CW, μm (in.)
0.3% at 3 days	5	2	24 (0.00094)	40 (0.0016)
0.5% at 3 days	9	6	29 (0.0011)	50 (0.002)
1.0% at 3 days	19	11	29 (0.0011)	60 (0.0024)
2.0% at 3 days	27	21	35 (0.0014)	80 (0.0031)
0.3% at 90 days	6	6	14 (0.00055)	30 (0.0012)
0.5% at 90 days	9	9	13 (0.00052)	40 (0.0016)
1.0% at 90 days	24	17	15 (0.00059)	50 (0.002)
2.0% at 90 days	50	29	18 (0.00071)	70 (0.0028)

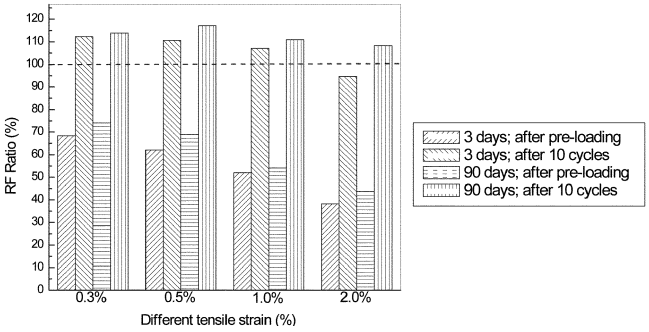

Fig. 2—RF recovery of self-healed ECC at different preloading after 10 wet-dry conditioning cycles. 100% indicates RF value of undamaged specimen.

As shown in Fig. 2, after preloading, the RF values are 38 to 69% of their initial RF for the 3-day-old specimens, recovering to between 94 and 113% of their initial RF after 10 wet-dry cycles. For 90-day-old specimens, the RF values are 43 to 74% of their initial RF after preloading and recover to between 108 and 113% after 10 wet-dry cycles. A higher tensile strain leads to a higher loss of RF and less RF recovery. Ninety-day-old specimens have both less RF loss and more RF recovery than 3-day-old samples at identical preloading levels. Although younger samples have more unhydrated cement, and therefore a higher capacity for self-healing, older samples have an improved fiber/matrix interfacial bond. Therefore, cracking is better distributed and the cracks are finer, which facilitates self-healing (Table 3). In addition, most samples (except for the 3-day-old specimen with 2.0% strain preloading), recover more than 100% of their initial RF after 10 wet-dry cycles.

Aside from self-healing, other possible sources for RF increase include moisture content changes and/or further hydration for specimens exposed to the wet-dry cycling regimes. In Fig. 3, the RF ratio of the control specimens (without preloading and therefore no crack damage) reveals the influence of the wet-dry cycles on the specimen RF; it is clear that the continued hydration/moisture increase in the bulk material during conditioning causes an increase in RF. This influence is stronger for the 3-day-old specimens due to the presence of a larger number of unhydrated cement grains.

To remove the effect of further hydration and/or moisture content changes on RF value improvement and to investigate the true extent of RF recovery due to self-healing, the normalized RF was calculated based on the following

$$\text{Normalized RF} = \frac{RF_{preload,\,condition}}{RF_{virgin,\,condition}} \times 100\% \qquad (2)$$

where $RF_{preload,\,condition}$ is the RF value of preloaded specimens that underwent wet-dry cycles and $RF_{virgin,\,condition}$ is the RF value of control virgin specimens that underwent the same conditioning but without preloading. The RF ratio thus calculated removes the effect of further hydration and/or moisture content on the bulk material that occurs in the preloaded and virgin specimens. A normalized RF of 100% implies a full recovery from crack damage. Note that the presence of microcracks may allow improved hydration of bulk materials adjacent to the crack walls. This effect, which is assumed to be small, is not accounted for in this study.

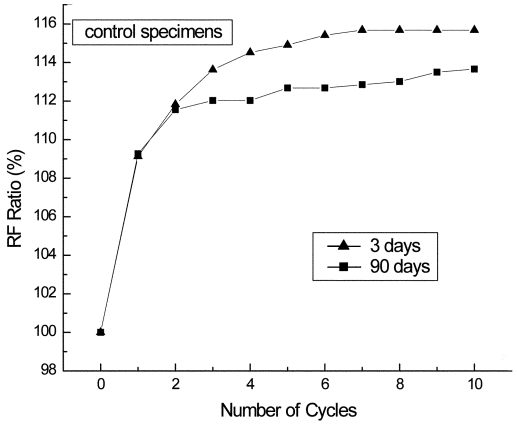

Fig. 3—Influence of continued hydration and moisture increase on increase of RF for bulk material (control specimens without cracks).

The effect of the number of wet-dry cycles on changes in RF is summarized in Fig. 4. The normalized RF for specimens preloaded to strain levels of 0.3%, 0.5%, 1.0%, and 2.0% after 3 and 90 days of aging are shown in Fig. 4(a) through (d), respectively, as a function of the number of conditioning cycles. After removing the influence of hydration/moisture, RF recovery that can be attributed to self-healing is still evident. Therefore, wet-dry cycles contribute to the self-healing of crack-damaged ECCs. Most RF improvement happens before four to five cycles, after which additional increases level off. After 10 wet-dry cycles, the normalized RF regains nearly 100% for 0.3 and 0.5% preload strain, 95% for 1.0% preload strain, and 90% for 2.0% preload strain for 90-day-old specimens.

Regarding the effect of age, the 90-day-old samples had a slightly higher RF recovery compared to the 3-day-old specimens. This is likely due to the fact that cracks in the 90-day-old specimens were on average smaller—even though there was a larger number of them—than those in the 3-day-old specimens. These tighter cracks are more easily filled with healing products.

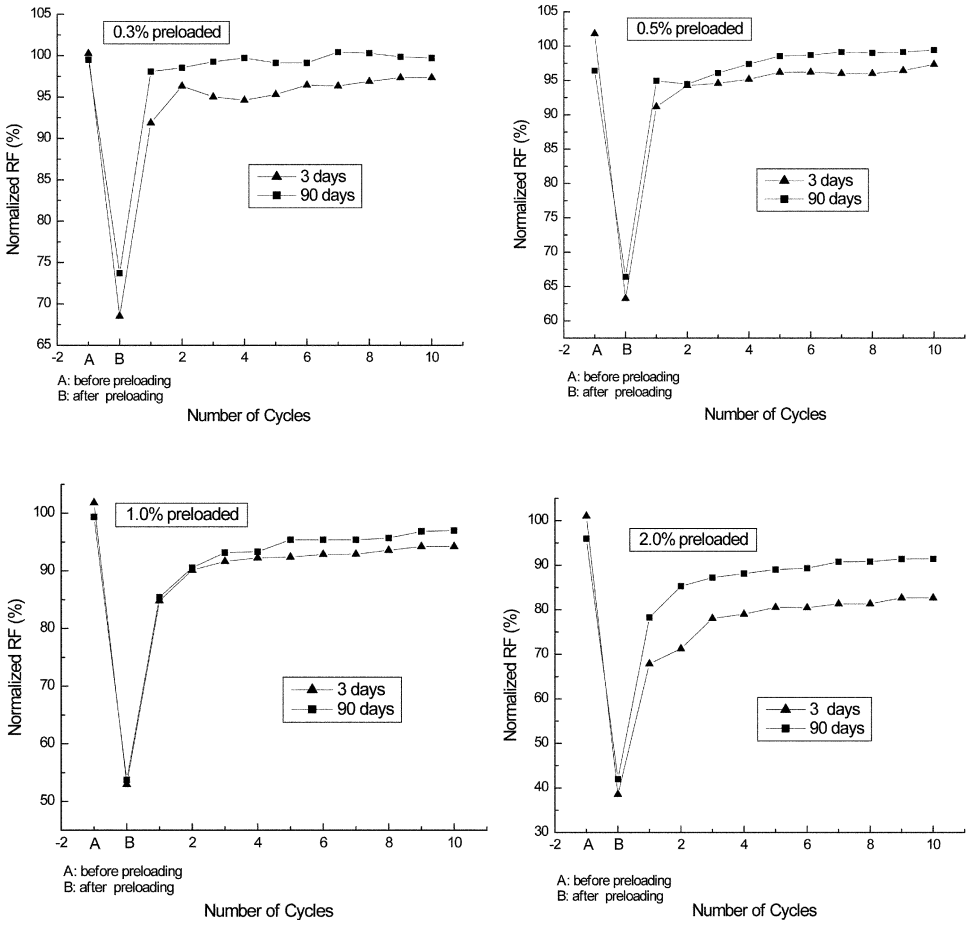

Fig. 4—True extent of RF recovery of 3- and 90-day-old ECC under wet-dry cycles for different preload strain levels.

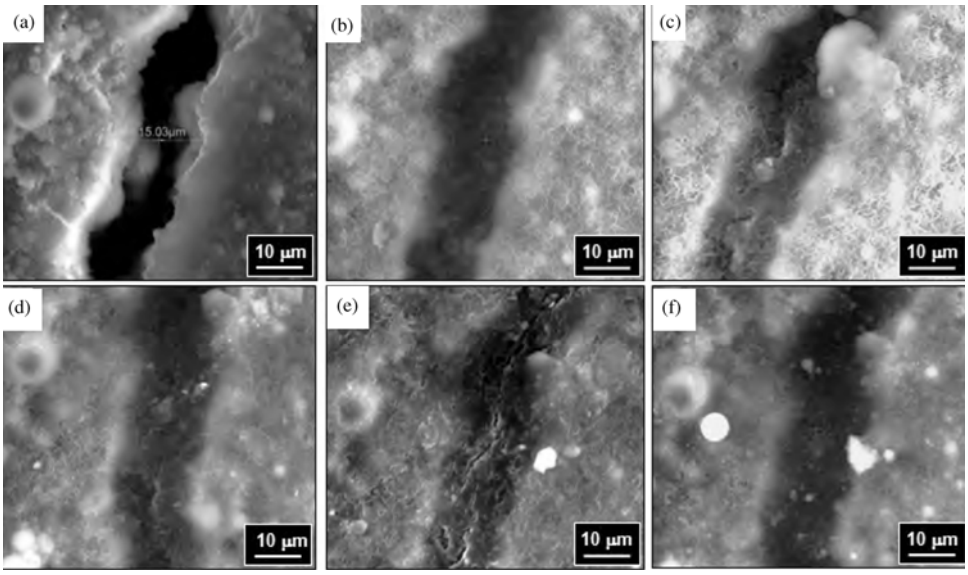

Fig. 5—ESEM images of self-healing process in ECC (15 μm CW): (a) before self-healing (0 cycles); (b) after one cycle; (c) after three cycles; (d) after 10 cycles; (e) after 20 cycles; and (f) after 49 cycles.

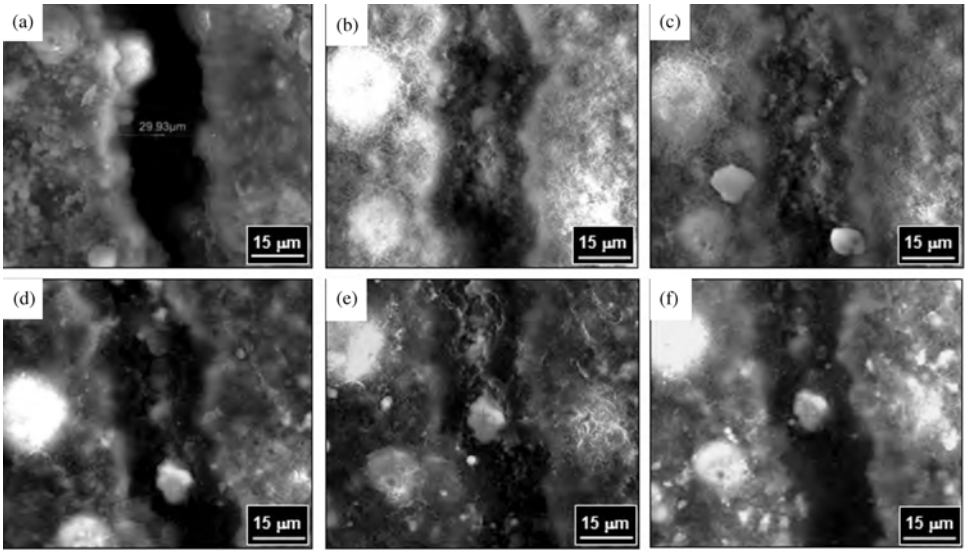

Fig. 6—ESEM images of self-healing process in ECC (30 μm CW): (a) before self-healing (0 cycles); (b) after one cycle; (c) after three cycles; (d) after 10 cycles; (e) after 20 cycles; and (f) after 49 cycles.

Morphology of self-healing products in ECC

To characterize the self-healing process, samples were observed by ESEM. Only the 90-day-old specimens were studied. After preloading, a 10 x 10 x 10 mm (0.4 x 0.4 x 0.4 in.) cube was cut from a tensile coupon. The ESEM allows continuous imaging during the healing processes because no special coating is required. In addition, the ESEM operates under variable pressure conditions that do not require a high vacuum, which could possibly alter the specimen. After imaging, the cube specimens were placed in water, then removed for imaging, and then replaced in water until they experienced 49 wet-dry cycles.

The growth processes of self-healing products on 15 μm, 30 μm, and 50 μm cracks, as well as on fiber surfaces, are displayed in Fig. 5 to 7, respectively. After the first wet-dry conditioning cycle, some self-healing products were already evident in all of the cracks. For the 15 μm cracks, fiber-like self-healing products were observed growing from both sides of the crack surface until they eventually met. After additional wet-dry cycles, the fiber-like self-healing products became much denser, and after 49 cycles, the crack was almost completely filled. For 30 μm cracks, stone-like particles were observed growing under the fiber-like self-healing products after one wet-dry cycle. These stone-like particles were not observed in the smaller cracks. After further wet-dry cycles, the fiber-like self-healing product became much denser and continued to grow from both sides, almost fully bridging the crack. After 49 cycles, some stone-like self-healing products were still observed on the crack surface. Regarding 50 μm cracks, a few fiber-like products were observed growing from either side of the crack; they

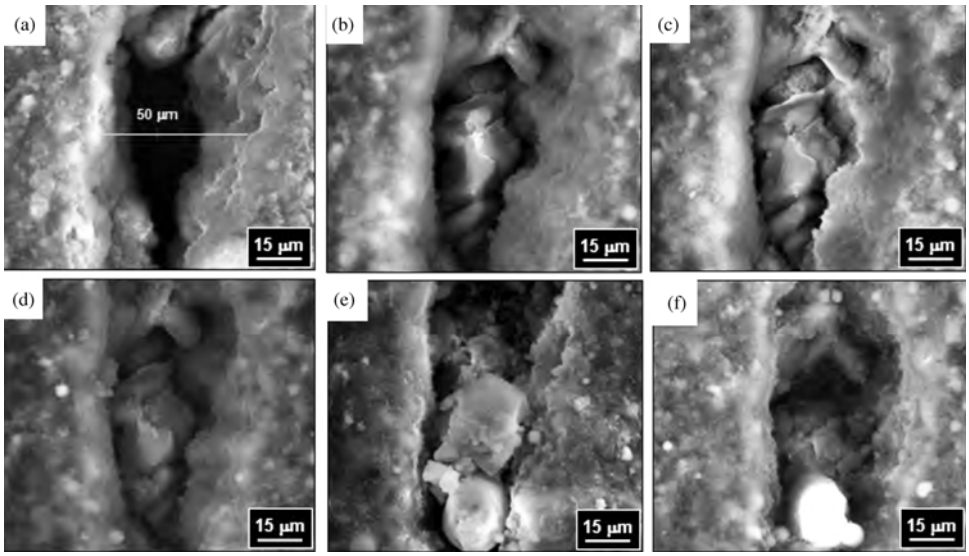

Fig. 7—ESEM images of self-healing process in ECC (50 μm CW): (a) before self-healing (0 cycles); (b) after one cycle; (c) after three cycles; (d) after 10 cycles; (e) after 20 cycles; and (f) after 49 cycles.

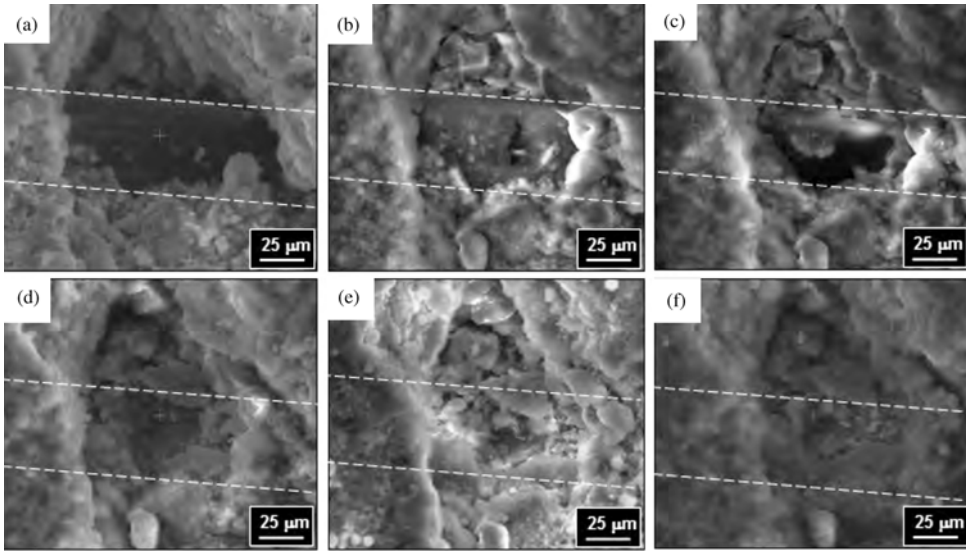

Fig. 8—ESEM images of self-healing process in ECC on fiber surface: (a) before self-healing (0 cycles); (b) after one cycle; (c) after three cycles; (d) after 10 cycles; (e) after 20 cycles; and (f) after 49 cycles.

were unable, however, to fully bridge the crack. Some stone-like particles were also observed in the crack; incomplete healing, however, was evident after 49 cycles.

In summary, a fiber-like phase is the main self-healing product in 15 μm cracks; both fiber-like and stone-like particles were observed in 30 μm cracks; and less self-healing product was observed in 50 μm cracks. It is possible that the stone-like particles required a minimum amount of space for growth, preventing their nucleation in the 15 μm cracks, but it is possible that they were too small to be observed by ESEM.

In addition to the crack surfaces, the crack-bridging PVA fibers themselves provided nucleation sites for healing products. As shown in Fig. 8, many fiber-like healing products were observed growing on the surface of the PVA fibers. After 10 wet-dry cycles, these products made it difficult to distinguish the PVA fibers from the matrix. The growth of healing products on the surface of PVA fibers may be due to the hydrophilic nature of the PVA surface and/or the presence of –OH groups, making it easier to form $Ca(OH)_2$.

Chemical characterization of healing products

EDS—To investigate the chemical nature of the self-healing products, specimens were examined using EDS. During ESEM observation, fiber-like products (Fig. 9(a)) and stone-like products (Fig. 9(b)) were distinct. At least three different points were analyzed by EDS for each product. Based on Table 4, the Ca:Si ratio of the fiber-like product is 2.07, and the O:Ca ratio of the stone-like product is approximately 3.62. These results suggest that the fiber-like self-healing may be C-S-H gel and the stone-like

Table 4—EDS element analysis of self-healing product A (fiber-like) and B (stone-like)*

Element	A (at. %)	B (at. %)
C	0	9.6 ± 0.9
O	72.9 ± 0.8	62.5 ± 0.3
Mg	10.3 ± 0.4	5.1 ± 0.4
Al	2.8 ± 0.1	2.1 ± 0.1
Si	4.4 ± 0.3	2.7 ± 0.1
Ca	9.1 ± 0.6	17.3 ± 0.8

*Elements with less than 1 atomic percent concentration not shown.

product may be $CaCO_3$; however, the presence of a mixed C-S-H/$Ca(OH)_2$ system in the former (which does not contain carbon) and a mixed C-S-H/$Ca(OH)_2$/$CaCO_3$ system in the latter (which contains an abundance of calcium) is difficult to rule out due to the limitations of EDS. Specifically, the interaction volume between the electron beam and the sample may be on the order of 1 μm^3 so that information from neighboring phases can bleed into each other. That the stone-like product does contain some carbonation product makes the presence of at least some $CaCO_3$ likely.

It should also be noted that many of the points in the fiber-like product contained a large amount of magnesium (~ 10 atomic %). The reason for this is not clear, as neither the raw materials nor unhealed ECC contain appreciable levels of magnesium. The most likely source of the magnesium is therefore the water that was used for the wet-dry cycles; however, no appreciable amounts of chlorine were detected. Possible dispositions of the magnesium include magnesium carbonate (magnesite), magnesium/calcium carbonate (dolomite), magnesium carbonate hydrates (barringtonite), or magnesium hydroxide (brucite.) Magnesium compounds are not mentioned in the self-healing literature and will be investigated further in future work.

XRD and FTIR test results—To complement the ESEM-EDS results, both FTIR and XRD experiments were performed. These tests were carried out because identification of the chemical nature of the self-healing compounds will be essential to future attempts to develop robust self-healing materials. As shown in Fig. 9(c), the rehealing products can be observed by the naked eye, occurring as white precipitates in the cracks. A small amount of this white healing material scratched from the sample was observed by TEM. The particle shown in Fig. 9(d) was confirmed by TEM-EDS to be $CaCO_3$.

X-ray diffractograms of several materials involved in this study (Fig. 10(a)) show well-defined peaks. Sand and fly ash (components of ECC) contain mainly quartz. The diffractogram of a control specimen—from preloaded ECC that did not undergo healing—contained quartz and some calcite. The diffractograms of specimens taken by drilling into the bulk with a small drill bit appear similar, though the peaks related to calcite are better defined. Due to the size of the (relatively large) drill bit compared to the size of the (relatively small) microcrack, the powder obtained in this manner is a mixture of both the healing product and the surrounding cementing phase. Three specimens obtained in this way were identical (thus, only one is plotted in Fig. 10(a)). Finally, powder was obtained by using a razor to scratch the healing product. As this scratching produced much less material than the drilling method, it was performed on the largest cracks. Due to the more precise scratching, the amount of the surrounding cementing phase included was reduced. Two diffractograms obtained were identical, and though some quartz is still evident, the majority of peaks are related to calcite. Overall, these results indicate that calcite is the primary crystalline product involved in the healing process.

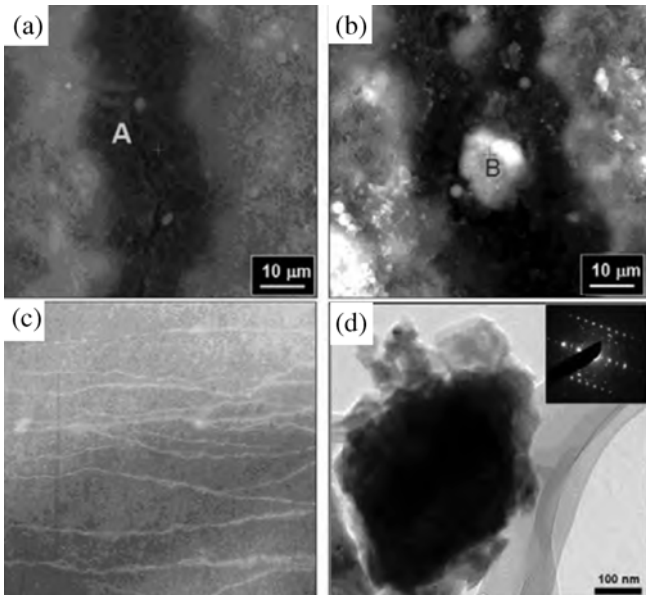

Fig. 9—(a) ESEM image of fiber-like healing product; (b) ESEM image of stone-like healing product; (c) self-healing ECC specimen surface after 10 wet-dry cycles (3-day-old; 1% preload strain); and (d) TEM image of healing product scraped from surface.

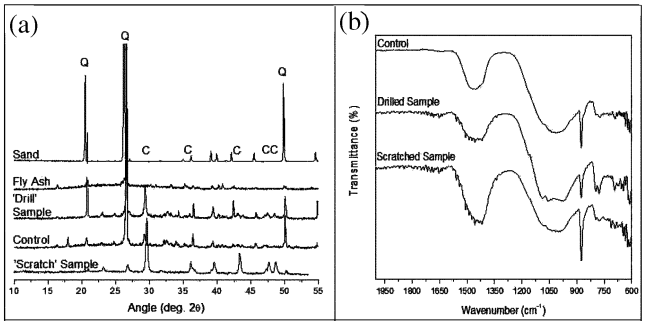

Fig. 10—(a) XRD diffractograms; and (b) FTIR spectra of self-healing products in ECC.

FTIR spectra (Fig. 10(b)) were collected from three similar specimens: a control sample of ECC that did not undergo healing cycles, a sample obtained by drilling as described in the XRD analysis section, and a sample obtained by scratching the healing product with a razor. The scratched sample is the most representative of pure healing material, whereas the drilled sample also contains some of the material surrounding the crack.

The three spectra share a number of similarities. A wide peak from roughly 1350 to 1550 cm^{-1} is representative of the stretching vibrations of CO_3^{2-}, though the origin of the peak ($CaCO_3$ versus $MgCO_3$) is not specified. The bending vibrations of this ion are also the source of the sharp peak near 875 cm^{-1}. These two peaks indicate the presence of $CaCO_3$ in the form of calcite.

A very wide, poorly defined peak from roughly 900 to 1100 cm^{-1} is representative of a variety of silicate stretching modes. A very weak triplet of peaks at 790, 780, and 690 cm^{-1} are indicative, when taken together, of quartz (from either the sand or fly ash used in the ECCs). These three peaks, though weak, are most well-defined in the spectrum of the drilled sample. Finally, the noise at the ends of the spectra (greater than approximately 1500 cm^{-1} and less than 700 cm^{-1}) is due to the presence of atmospheric water vapor. The peaks due to atmospheric CO_2 (not shown) are quite minor and are not sufficiently intense to account for the bonds attributed to calcite here.

The poorly defined peak due to silicate bonding was the main difference between the spectra. First, this peak is somewhat less intense in the scratched sample, implying that the bulk of the healing product is calcite. Second, in the drilled sample, rather than being a single, wide peak, it has three minima at 1090, 1060, and 970 cm^{-1}. It is possible that this occurred because CO_2 was leaching Ca from the surrounding C-S-H rather than consuming CH to create calcite. When this happens, the Si in the C-S-H becomes more highly polymerized, which in turn leads to the well-known phenomenon of FTIR peaks shifting to higher wave numbers.

CONCLUSIONS

The self-healing behavior and process of high-tensile ductility ECCs have been investigated in this paper. The observation of crack characteristics at 0.3, 0.5, 1.0, and 2.0% preloading, RF recovery behavior, ESEM observations, and EDS/TEM/FTIR/XRD analyses are reported. These results suggest that ECC, which is tailored for high-tensile ductility and self-controlled CW, has many characteristics that contribute to self-healing behavior. The tight CW of ECCs is illustrated by a maximum CW of less than 80 μm even with 2.0% tensile strain damage. CW of less than 50 μm leads to highly robust self-healing. Compared to 3-day-old samples, 90-day-old samples had many more cracks of smaller width—a prime condition for self-healing—which leads to slightly better RF recovery. Wet-dry cycles contributed to the self-healing of ECCs, as evidenced by rapid RF recovery after four to five cycles. After 10 wet-dry cycles, RF recovery due to self-healing exceeded 90%, even at a 2.0% imposed strain.

The self-healing products have been confirmed by the complementary use of EDS, TEM, FTIR, and XRD to be fiber-like C-S-H and stone-like $CaCO_3$, varying by CW. C-S-H is the main self-healing product for CWs of 15 μm, and C-S-H and $CaCO_3$ are the main self-healing products for CWs of 30 μm. Less self-healing product is seen at CWs of 50 μm; however, below this width, cracks can be almost completely healed. Further hydration and the formation of $CaCO_3$ crystals are the main reasons for the self-healing phenomena. Finally, PVA fibers in ECC provide nucleation sites for healing products that may aid in the self-healing of ECCs.

ACKNOWLEDGMENTS

This research was partially funded by an NSF Civil Infrastructure Grant CMMI 0700219 and a China National Scholarship that supports the first author as a Visiting Scholar at the University of Michigan. The authors wish to thank the Holcim Co., the Boral Co., U.S. Silica, Kuraray Co., and W.R. Grace & Co. for providing Type I ordinary portland cement, fine silica sand, Class F normal fly ash, PVA fibers, and HRWRA, respectively.

REFERENCES

1. Jacobsen, S.; Marchand, J.; and Gerard, B., "Concrete Cracks I: Durability and Self-Healing—A Review," *Proceedings of the 2nd International Conference on Concrete under Severe Conditions, Environment and Loading*, V. 1, O. E. Gjorv et al., eds., E&FN Spon, Tromso, Norway, 1998, pp. 217-231.

2. Kenneth, R. L., and Floyd, O. S., "Autogenous Healing of Cement Paste," ACI JOURNAL, *Proceedings* V. 52, No. 6, June 1956, pp. 52-63.

3. Edvardsen, C., "Water Permeability and Autogenous Healing of Cracks in Concrete," *ACI Materials Journal*, V. 96, No. 6, Nov.-Dec. 1999, pp. 448-455.

4. Ripphausen, B., "Investigations of the Water Permeability and Repair of Reinforced Concrete Structures with Through Cracks," PhD thesis, RWTH Aachen, Aachen, Germany, 1989. (in German)

5. Granger, S.; Loukili, A.; Pijaudier-Cabot, G.; and Chanvillard, G., "Experimental Characterization of the Self-Healing of Cracks in an Ultra-High-Performance Cementitious Material: Mechanical Tests and Acoustic Emission Analysis," *Cement and Concrete Research*, V. 37, No. 4, Apr. 2007, pp. 519-527.

6. Wang, K.; Jansen, D.; Shah, S.; and Karr, A., "Permeability Study of Cracked Concrete," *Cement and Concrete Research*, V. 27, No. 3, Mar. 1997, pp. 381-393.

7. Li, V. C., *ECC—Tailored Composites through Micromechanical Modeling, Fiber Reinforced Concrete: Present and the Future*, N. Banthia et al., eds., CSCE, Montreal, QC, Canada, 1998, 64 pp.

8. Li, V. C., "On Engineered Cementitious Composites (ECC)—A Review of the Material and Its Applications," *Journal of Advanced Concrete Technology*, V. 1, No. 3, 2003, pp. 215-230.

9. Wang, S., "Micromechanics Based Matrix Design for Engineered Cementitious Composites," PhD dissertation, Department of Civil and Environmental Engineering, University of Michigan, Ann Arbor, MI, 2005, 222 pp.

10. Li, V. C., "From Micromechanics to Structural Engineering—The Design of Cementitious Composites for Civil Engineering Applications," *Journal of Structural Mechanics and Earthquake Engineering*, JSCE, V. 10, No. 2, 1993, pp. 37-48.

11. Maalej, M.; Hashida, T.; and Li, V. C., "Effect of Fiber Volume Fraction on the Off-Crack Plane Energy in Strain-Hardening Engineered Cementitious Composites," *Journal of the American Ceramics Society*, V. 78, No. 12, 1995, pp. 3369-3375.

12. Li, V. C., and Yang, E. H., *Self Healing Materials: An Alternative Approach to 20 Centuries of Materials Science*, Springer, Dordrecht, the Netherlands, 2007, 221 pp.

13. Yang, Y. Z.; Lepech, M.; Yang, E. H.; and Li, V. C., "Autogenous Healing of Engineered Cementitious Composites under Wet-Dry Cycles," *Cement and Concrete Research*, V. 39, 2009, pp. 382-390.

14. Ismail, M.; Toumi, A.; Francois, R.; and Gagne, R., "Effect of Crack Opening on Local Diffusion of Chloride Inert Materials," *Cement and Concrete Research*, V. 34, No. 4, Apr. 2004, pp. 711-716.

15. Hearn, N., "Self-Sealing, Autogenous Healing and Continued Hydration: What is the Difference?" *Materials and Structures*, V. 31, No. 8, Oct. 1998, pp. 563-567.

16. Reinhardt, H., and Joos, M., "Permeability and Self-Healing of Cracked Concrete as a Function of Temperature and Crack Width," *Cement and Concrete Research*, V. 33, No. 7, July 2003, pp. 981-985.

17. Termkhajornkit, P.; Nawa, T.; Yamashiro, Y.; and Saito, T., "Self-Healing Ability of Fly Ash-Cement Systems," *Cement and Concrete Composites,* V. 31, No. 3, Mar. 2009, pp. 195-203.

18. Ter Heide, N., "Crack Healing in Hydrating Concrete," master's dissertation, Delft University of Technology, Delft, the Netherlands, 2005.

19. Neville, A., "Autogenous Healing—A Concrete Miracle?" *Concrete International*, V. 24, No. 11, Nov. 2002, pp. 76-82.

20. Li, V. C.; Wang, S.; and Wu, C., "Tensile Strain-Hardening Behavior of PVA-ECC," *ACI Materials Journal*, V. 98, No. 6, Nov.-Dec. 2001, pp. 483-492.

21. Li, V. C.; Wu, C.; Wang, S.; Ogawa, A.; and Saito, T., "Interface Tailoring for Strain-Hardening PVA-ECC," *ACI Materials Journal*, V. 99, No. 5, Sept.-Oct. 2002, pp. 463-472.

22. Wang, S., and Li, V. C., "Polyvinyl Alcohol Fiber Reinforced Engineered Cementitious Composites: Material Design and Performance," *Proceedings of International RILEM Workshop on HPFRCC in Structural Applications*, G. Fischer and V. C. Li, eds., Honolulu, HI, 2005, pp. 65-74.